Dynamic Evolution of Fermion Parity in the Kitaev Honeycomb Model

Demetris Demetriades
Department of physics
University of Athens
dd97867427@gmail.com
sph2100190@uoa.gr

Abstract

We investigate the dynamic evolution of fermionic parity in the Kitaev honeycomb model (HKM) through a combination of analytical derivation and large-scale computational experiments. Using a lattice of one hundred hexagonal plaquettes, we systematically study how local flux excitations $u_{ij} = -1$ affect the global fermionic parity $P = \text{sgn}(\text{Pf}(A))$ of the system. By fixing one reference bond ($u_{12} = -1$) and varying all other bonds sequentially, the objective of this study is to search for a global topological rule that describes how a local gauge variation u_{ij} can influence a global invariant such as the fermionic parity. Understanding this connection is essential for revealing how local gauge dynamics encode global topological properties and for predicting parity changes without the need for full Pfaffian evaluation—an advance that could significantly accelerate simulations and clarify the stability of Majorana-based quantum information. The numerical analysis reveals consistent geometrical patterns suggesting that parity changes depend not only on the number of flipped bonds but also on their spatial arrangement and bond orientation within the lattice. Although a precise mathematical law has not yet been formulated, the observed behavior points toward a deeper topological connection between local gauge dynamics and global parity sectors, which may motivate further analytical exploration by other researchers. The full computational framework (C++ generation of A-matrices, Pfaffian calculations, and data analysis scripts) is available at `github.com/dimis2/Dynamic-Evolution-of-Fermion-Parity-`.

Data and Code Availability

All source code, simulation scripts, and data are openly available at:
`github.com/dimis2/Dynamic-Evolution-of-Fermion-Parity-`.

1 Introduction

We begin by presenting a basic background on the Honeycomb Kitaev model (HKM), so that readers who are not familiar with it can follow and understand the sections of this paper. For those

who seek a deeper understanding of the model, we refer them to [1], [2]. The model features a honeycomb lattice structure, where each vertex hosts a particle with spin $\pm\frac{1}{2}$. The lattice is divided into two equivalent sublattices: the odd and the even (they are shown by empty and full circles in the figure). Depending on the direction of each bond, three distinct types of interactions arise—namely, x-, y-, and z-links.

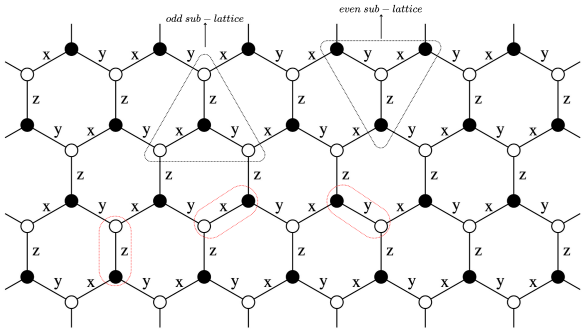

Figure 1: Geometry of the honeycomb model, where we present the two equivalent sublattices (even and odd) and the three types of interactions (x-, y-, z-links), depending of the direction of each bond.

The Hamiltonian of the system is defined as:

$$\mathcal{H} = -J_x \sum_{\text{x-links}} \sigma_i^x \sigma_j^x - J_y \sum_{\text{y-links}} \sigma_i^y \sigma_j^y - J_z \sum_{\text{z-links}} \sigma_i^z \sigma_j^z, \tag{1}$$

where J_x, J_y, and J_z are coupling constants that describe the strength of the interaction along the x-, y-, and z-bonds of the lattice.
The representation of spins in the extended space $\tilde{\mathcal{L}}$ is achieved using four Majorana operators, γ^x, γ^y, γ^z, and γ, which we represent as dots.

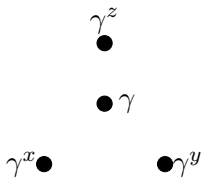

The spin operator takes the form $\tilde{\sigma}_j^{\alpha_i} = i\,\gamma_j^{\alpha_i}\gamma_j$, where $(\alpha_i = x, y, z)$ depends on the direction of each bond. The Hamiltonian in space $\tilde{\mathcal{L}}$ using majorana formalism defined as:

$$\tilde{\mathcal{H}} = \frac{i}{4}\sum_{\langle j,k\rangle} \hat{A}_{jk}\gamma_j\gamma_k, \quad A_{jk} = \begin{cases} 2J_{\alpha_{jk}}\hat{u}_{jk}, & \text{if } j \text{ are } k \text{ connected,} \\ 0, & \text{otherwise.} \end{cases} \tag{2}$$

We define the bond operator as $\hat{u}_{jk} = i\gamma_j^{\alpha_i}\gamma_k^{\alpha_i}$ (see Fig. 2), which is antisymmetric, i.e., $u_{jk} = -u_{kj}$. The only possible eigenvalues of the operator u_{jk} are ± 1. We are now ready to partition the

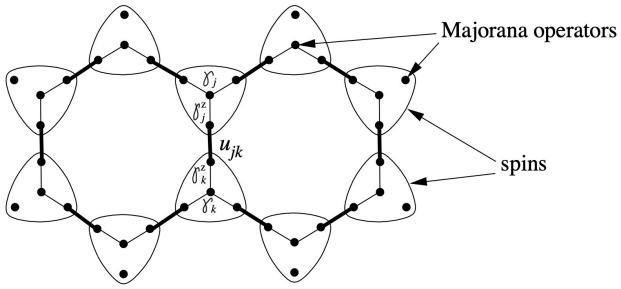

Figure 2: Graphical representation of the Hamiltonian, as given in eq. (2). Each spin corresponds to four distinct dots, each representing a Majorana operator.

extended Hilbert space $\tilde{\mathcal{L}}$ of the system into sectors, where each sector corresponds to a distinct configuration of eigenvalues of the bond operator $\hat{u}_{jk}$:

$$\tilde{\mathcal{L}} = \bigoplus_{u} \tilde{\mathcal{L}}_u. \tag{3}$$

The flux operator for each plate takes the form:

$$w_{p_n} = \prod_{(j,k)\in \text{boundary}(p)} u_{jk}, \tag{4}$$

where ($j \in$ even sub-lattice , $k \in$ odd sub-lattice) We define the cbf through the operators $\chi^{\dagger}_{\langle ij\rangle_\alpha}$

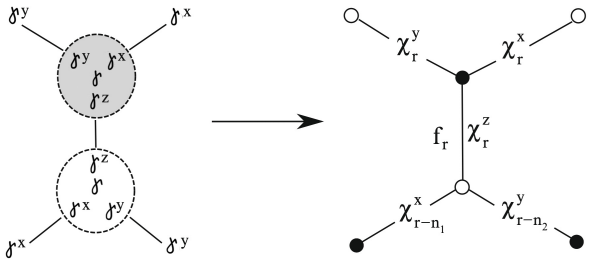

Figure 3: Graphical representation of complex bond and complex matter fermions (cbf and cmf)

and $\chi_{\langle ij\rangle_\alpha}$, which describe the state at the ends of the bond $\langle ij\rangle$, with the index α indicating the direction of the bond:

$$\chi_{\langle ij\rangle_\alpha} = \frac{1}{2}\left(\gamma_i^\alpha - i\gamma_j^\alpha\right), \quad \chi^{\dagger}_{\langle ij\rangle_\alpha} = \frac{1}{2}\left(\gamma_i^\alpha + i\gamma_j^\alpha\right) \tag{5}$$

We define the cmf through the operators f_r and $f_r^\dagger$, which describe the connections of central

Majorana fermions from sub-lattice A (even) to sub-lattice B (odd):

$$f_r = \frac{1}{2}\left(\gamma_{A,r} + i\gamma_{B,r}\right), \quad f_r^\dagger = \frac{1}{2}\left(\gamma_{A,r} - i\gamma_{B,r}\right). \tag{6}$$

eq. (2), in the cmb and cmf basis, takes the form:

$$\tilde{\mathcal{H}} = \frac{1}{2}\begin{pmatrix} f_r^\dagger & f_r \end{pmatrix}\begin{pmatrix} h & \Delta \\ \Delta^\dagger & -h^T \end{pmatrix}\begin{pmatrix} f_r \\ f_r^\dagger \end{pmatrix}, \tag{7}$$

$$\downarrow \quad \text{FT}$$

$$\tilde{\mathcal{H}}_0 = \begin{pmatrix} f_q^\dagger & f_{-q} \end{pmatrix}\begin{pmatrix} h_q & -\Delta_q \\ -\Delta_q^* & -h_q \end{pmatrix}\begin{pmatrix} f_q \\ f_{-q}^\dagger \end{pmatrix}. \tag{8}$$

We apply the BdG tranformation:

$$T^\dagger \mathcal{H}_{BdG} T = \begin{pmatrix} |S_q| & 0 \\ 0 & -|S_q| \end{pmatrix}.$$

Under the BdG tranformation the eq. (7) define as:

$$\tilde{\mathcal{H}}_0 = \sum_q |S_q|(2\alpha_q^\dagger \alpha_q - 1), \tag{9}$$

where $S_{\mathbf{q}} = \sum_{\mathbf{n}_i} J_{\alpha_{\mathbf{n}_i}} e^{i\mathbf{q}\cdot\mathbf{n}_i}$ encodes the coupling constants in momentum space. The vectors $\mathbf{n}_1 = \mathbf{n}_x = \left(\frac{1}{2}, \frac{\sqrt{3}}{2}\right)$, $\mathbf{n}_2 = \mathbf{n}_y = \left(-\frac{1}{2}, \frac{\sqrt{3}}{2}\right)$, $\mathbf{n}_3 = \mathbf{n}_z = (0,0)$ are expressed in units of the bond length and describe the relative positions of neighboring sites in the honeycomb lattice. The ground state energy of eq. (9) is $E_{g.s} = \langle \mathcal{M}_0 | \tilde{\mathcal{H}}_0 | \mathcal{M}_0 \rangle = -\sum_q |S_q|$. By varying the parameters J_x, J_y, and J_z in eq. (9), we compute all possible phases of the system, which are summarized in the phase diagram:

Suppose we wish to find the absolute minimum of the system. To achieve this, we would need to compare all values of $E_{\text{g.s.}}$ across all possible flux sectors. This is practically impossible. Fortunately, due to the translational symmetry of the system, we know that the ground state appears in the zero-flux sector, i.e., when all plates have eigenvalue $w_{p_i} = +1$. Although all plates share the same eigenvalue $+1$, the configuration of the local bond variables corresponding to each w_{p_i} is not necessarily the same (see eq. (4)), and therefore the terms in the sum $E_{\text{g.s.}}$ may differ from plate to plate. We assume the system is at low temperature, where all plates exhibit the same local configuration $u_{\langle ij \rangle} = +1$. The zero-flux state is denoted $|\mathcal{G}^0\rangle$, and the corresponding ground state of the cmf is denoted $|\mathcal{M}_0\rangle$. The probability for a bond $u_{\langle ij \rangle}$ to change follows the Boltzmann distribution:

$$P \sim e^{-\Delta_{\text{flux}}/k_B T}. \tag{10}$$

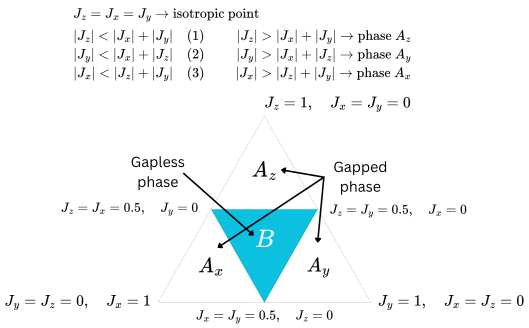

Figure 4: Phase diagram of the Kitaev model in the parameter space (J_x, J_y, J_z). The regions A_{α_i} correspond to gapped phases, while region B is gapless. Each point inside the triangle represents a specific combination of the couplings J_x, J_y, and J_z. The center of the triangle corresponds to the isotropic point. When all three triangle inequalities are satisfied, the system is in the gapless phase B. If one of the inequalities (1), (2), or (3) is violated, the system transitions to the corresponding gapped phase A_{α_i}, depending on which inequality is no longer satisfied.

For low temperatures ($k_B T \ll \Delta_{\text{flux}}$), the probability for a bond to change is exponentially small. **In the current paper, we consider the thermal fluctuations that occur in the system, which translate into local fluxes, i.e., $u_{ij} = -1$. Our goal is to examine how the variation of a local quantity u_{ij} can affect the fermionic parity, a global property of the system.** The fermionic parity in the honeycomb Kitaev model defined as:

$$P = \text{sgn}(\text{Pf}(A)), \tag{11}$$

where A is the matrix of eq. (2). In the HKM, eq. (11) determines whether the occupation number of the cmf in the ground state is even or odd:

$$P = (-1)^{N_f} = \begin{cases} +1, \text{ even occupation number of cmf} \\ -1, \text{ odd occupation number of cmf,} \end{cases}, \tag{12}$$

where N_f is the number of cmf. In the ground-state flux sector, $P = +1$ always. When a u_{ij} is changed (e.g., a flip on a boundary x-bond), the entire flux sector is altered. The new ground state of the system, with the updated u_{ij} configuration, is not the same as the previous one, as it has a different reference filling for the matter fermions. In the new gauge field, the set of occupied single-particle levels in the cmf energy spectrum may differ by one fermion compared to the old state, resulting in a new ground state with a different fermionic parity. **Our goal is to identify certain topological rules that determine under which conditions local fluxes can flip the fermionic parity.**

2 Computational Implementation

In this chapter, we present the computational framework developed to extract the various experiments. The complete implementation is available in detail on my GitHub Repository We begin by generating the specific form of the lattice, as described in Subsection 1.1. Once the lattice configuration is defined, we created a program in C++ named A1_matrix.cpp, which constructs the antisymmetric matrix A. Using the A1_matrix.cpp program, we can compute the matrix A for any given flux sector. The resulting matrix is saved to a .txt file and then processed using the pfaffian_calc.py script written in Python, which computes the fermionic parity of the corresponding sector.

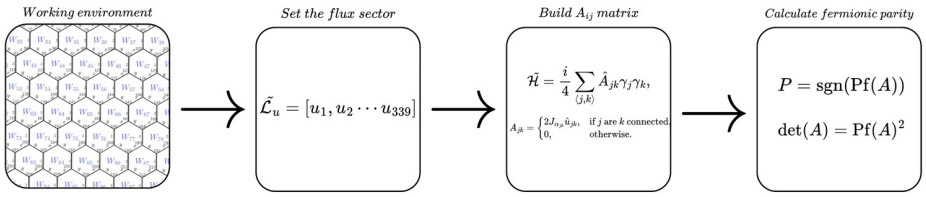

Figure 5: Visual representation of the computational framework

2.1 Working environment

In Fig. 5 we present the lattice on which the entire computational/experimental part is based. The lattice consists of 100 plates arranged in rows of ten. On each plate we indicate the plate index, the index of every site, and the orientation of every bond (x-, y-, or z-bond). Plates with zero flux are shown in blue, whereas plates carrying flux are shown in red. From the lattice geometry we have 339 local bonds u_{ij} and 240 sites. Consequently, the matrix A has dimension 240×240, i.e., $A \in \mathbb{R}^{240\times240}$.

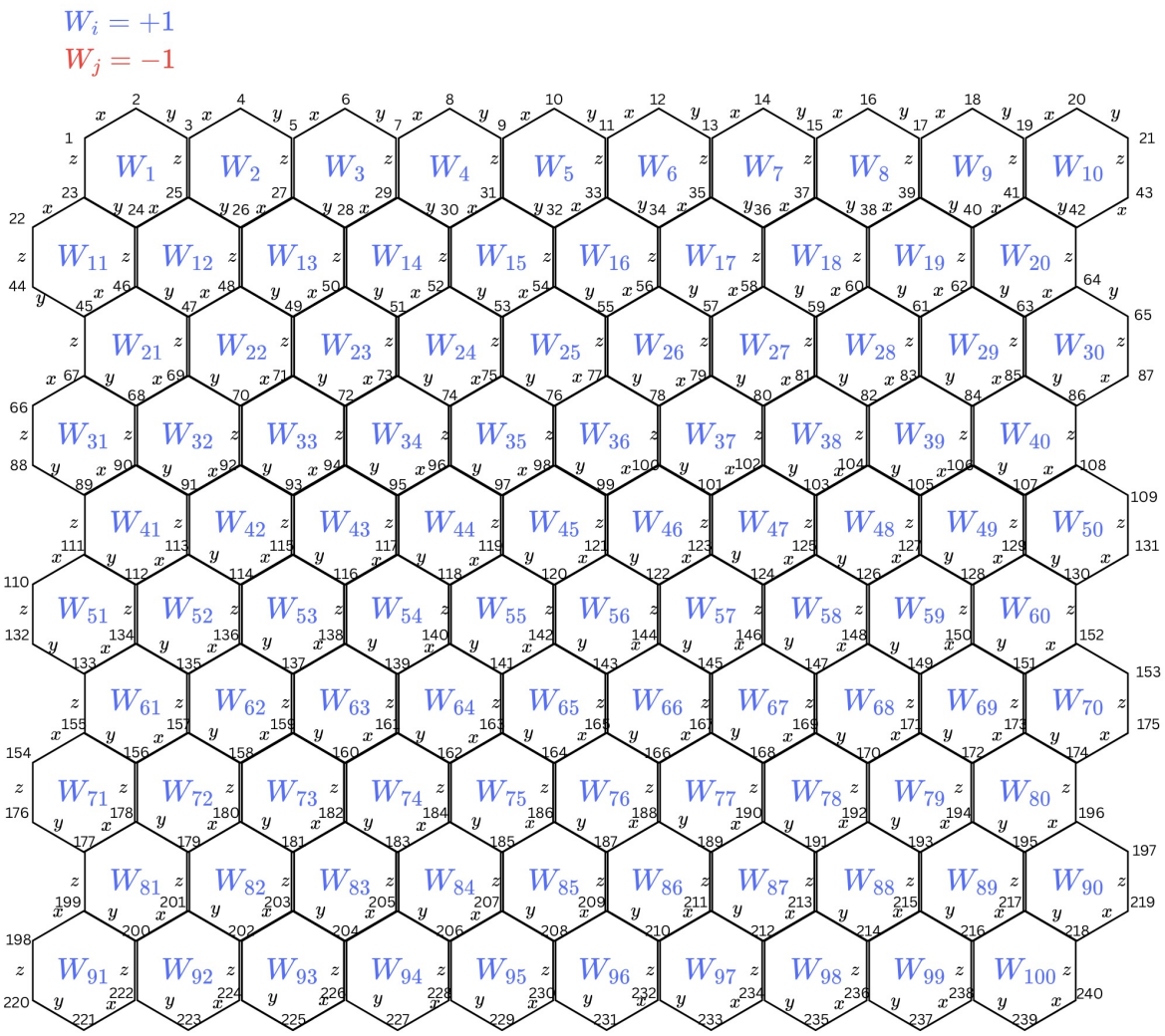

Figure 6: The HKM lattice for our experiments, which consists of 100 hexagonal plates $W_1 \dots W_{100}$, arranged in rows of 10. Each plate shows the orientation of the x, y, and z-type bonds, as well as the numbering of each site. Plates in blue correspond to zero flux ($W_i = +1$), while plates in red indicate the presence of flux ($W_j = -1$).

3 Explanation how measurements taken

We initially consider as a reference point the local bond with flux $u^x_{12} = -1$. The experimental procedure is divided into three experiments. We dynamically vary all local bonds with $u^x_{ij} = -1$ in

sequence and record the value of the parity. We then follow the same procedure for the local bonds u_{ij}^{y} and u_{ij}^{z}. Consequently, in each parity measurement there exist, throughout the entire lattice, only two local fluxes, u_{12}^{x} and u_{ij}^{α}. In Appendix A, we present in detail all the measurements for the three experiments separately, where the yellow line indicates the end of the sequence on the lattice.[1]. As can be observed, repeating patterns appear systematically along each row, separately for each experiment, which suggests that there exists a connection between the local flux on the lattice and a global variable such as the fermionic parity. Unfortunately, however, we were not able to establish a universal topological rule that demonstrates this connection.

[1] $u_{ij}^{\alpha}, \quad \alpha = x, y, z - bond$

References

[1] Demetris Demetriades. Review paper in honeycomb kitaev model – anyons in an exactly solved model and beyond, 2025. School of Science, Department of Physics, National and Kapodistrian University of Athens.

[2] Alexei Kitaev. Anyons in an exactly solved model and beyond. *arXiv preprint*, 2008.

A Measurements

Table 1: Results from the first experiment, where the yellow line indicates the end of the row in the lattice. $u^x_{ij} \equiv u_{ij}(x_{bond})$

$u^x_{ij} = -1$	$u^x_{ij} = -1$	parity
1 2	3 4	1
1 2	5 6	1
1 2	7 9	1
1 2	9 10	1
1 2	11 12	1
1 2	13 14	-1
1 2	15 16	-1
1 2	17 18	-1
1 2	19 20	-1
1 2	22 23	1
1 2	24 25	1
1 2	26 27	-1
1 2	29 28	-1
1 2	31 30	-1
1 2	33 32	-1
1 2	33 34	-1
1 2	37 36	1
1 2	39 38	1
1 2	41 40	1
1 2	43 42	1
1 2	45 46	-1
1 2	47 48	-1
1 2	49 50	1
1 2	51 52	1
1 2	53 54	1
1 2	56 55	1
1 2	58 57	-1
1 2	60 59	-1
1 2	62 51	-1
1 2	64 63	-1
1 2	60 67	1
1 2	69 68	1
1 2	70 71	-1
1 2	73 72	-1
1 2	75 74	-1
1 2	77 76	-1
1 2	79 78	-1
1 2	81 80	1
1 2	83 82	1
1 2	85 84	1
1 2	87 86	1
1 2	90 89	-1
1 2	91 92	-1
1 2	94 93	1
1 2	96 95	1
1 2	98 97	1
1 2	100 99	1
1 2	102 101	-1

Table 1: (continued)

$u_{ij}^x = -1$	$u_{ij}^x = -1$	parity
1 2	104 103	-1
1 2	106 105	-1
1 2	108 107	-1
1 2	110 111	1
1 2	113 112	1
1 2	115 114	-1
1 2	117 116	-1
1 2	119 118	-1
1 2	121 120	-1
1 2	123 122	-1
1 2	125 124	1
1 2	127 126	1
1 2	129 128	1
1 2	131 130	1
1 2	133 134	-1
1 2	135 136	-1
1 2	138 137	1
1 2	140 139	1
1 2	142 141	1
1 2	144 143	1
1 2	146 145	-1
1 2	148 147	-1
1 2	150 149	-1
1 2	152 151	-1
1 2	154 155	1
1 2	157 156	1
1 2	159 158	-1
1 2	161 160	-1
1 2	163 162	-1
1 2	165 164	-1
1 2	167 166	-1
1 2	169 168	1
1 2	171 170	1
1 2	173 172	1
1 2	175 174	1
1 2	178 177	-1
1 2	190 179	-1
1 2	182 181	1
1 2	184 183	1
1 2	186 185	1
1 2	188 187	1
1 2	190 189	-1
1 2	192 191	-1
1 2	194 193	-1
1 2	196 195	-1
1 2	198 199	1
1 2	201 200	1
1 2	203 202	1
1 2	205 264	-1
1 2	264 206	-1
1 2	211 210	-1
1 2	213 212	1

Table 1: (continued)

$u^x_{ij} = -1$	$u^x_{ij} = -1$	parity
1 2	215 214	1
1 2	217 216	1
1 2	219 210	1
1 2	222 221	-1
1 2	224 223	-1
1 2	226 225	-1
1 2	228 227	1
1 2	230 229	1
1 2	232 231	1
1 2	234 233	1
1 2	236 235	1
1 2	238 237	1
1 2	240 239	1

Table 2: Results from the second experiment, where the yellow line indicates the end of the row in the lattice. $u^y_{ij} \equiv u_{ij}(y_{bond})$

$u^x_{ij} = -1$	$u^y_{ij} = -1$	parity
1 2	2 3	-1
1 2	4 5	-1
1 2	6 7	-1
1 2	8 9	-1
1 2	10 11	-1
1 2	12 13	-1
1 2	14 15	1
1 2	16 17	1
1 2	18 19	1
1 2	20 21	1
1 2	24 23	-1
1 2	26 25	-1
1 2	28 27	-1
1 2	30 29	1
1 2	32 31	1
1 2	34 33	1
1 2	36 35	-1
1 2	38 37	-1
1 2	40 39	-1
1 2	42 41	-1
1 2	45 44	1
1 2	47 46	1
1 2	49 48	-1
1 2	51 50	-1
1 2	53 52	-1
1 2	55 54	-1
1 2	57 56	-1
1 2	59 58	1
1 2	61 60	1
1 2	63 62	1
1 2	68 67	1
1 2	70 69	1

Table 2: (continued)

$u_{ij}^{x} = -1$	$u_{ij}^{y} = -1$	parity
1 2	72 71	-1
1 2	74 73	-1
1 2	76 75	-1
1 2	78 77	-1
1 2	80 79	-1
1 2	82 81	1
1 2	84 83	1
1 2	86 85	1
1 2	89 98	-1
1 2	91 90	-1
1 2	93 92	1
1 2	95 94	1
1 2	97 96	1
1 2	99 98	1
1 2	101 100	-1
1 2	103 102	-1
1 2	105 104	-1
1 2	107 106	-1
1 2	112 111	1
1 2	114 113	1
1 2	116 115	-1
1 2	118 117	-1
1 2	120 119	-1
1 2	122 121	-1
1 2	124 123	-1
1 2	126 125	1
1 2	128 127	1
1 2	130 129	1
1 2	132 133	-1
1 2	135 134	-1
1 2	137 136	-1
1 2	139 138	1
1 2	141 140	1
1 2	143 142	1
1 2	145 144	-1
1 2	147 146	-1
1 2	149 148	-1
1 2	151 150	-1
1 2	155 156	1
1 2	158 157	1
1 2	160 159	-1
1 2	162 161	-1
1 2	164 163	-1
1 2	166 165	-1
1 2	168 167	-1
1 2	170 169	1
1 2	172 171	1
1 2	174 173	1
1 2	177 176	-1
1 2	179 178	-1
1 2	181 180	-1
1 2	183 182	1

Table 2: (continued)

$u^x_{ij} = -1$	$u^y_{ij} = -1$	parity
1 2	185 184	1
1 2	187 186	-1
1 2	189 188	-1
1 2	191 190	-1
1 2	193 192	-1
1 2	195 194	-1
1 2	200 199	-1
1 2	202 201	-1
1 2	204 203	-1
1 2	206 205	1
1 2	208 207	1
1 2	210 209	-1
1 2	212 211	-1
1 2	214 213	-1
1 2	216 215	-1
1 2	218 217	-1
1 2	221 220	1
1 2	223 222	1
1 2	225 224	1
1 2	227 226	-1
1 2	229 228	-1
1 2	231 230	-1
1 2	233 232	-1
1 2	235 234	-1
1 2	237 236	-1
1 2	239 238	-1

Table 3: Results from the third experiment, where the yellow line indicates the end of the row in the lattice. $u^z_{ij} \equiv u_{ij}(z_{bond})$

$u^x_{ij} = -1$	$u^z_{ij} = -1$	parity
1 2	3 25	-1
1 2	5 27	-1
1 2	7 29	-1
1 2	9 31	-1
1 2	11 33	-1
1 2	13 35	-1
1 2	15 37	-1
1 2	17 39	-1
1 2	19 41	-1
1 2	21 43	-1
1 2	44 22	-1
1 2	24 46	-1
1 2	26 48	-1
1 2	28 50	-1
1 2	30 52	-1
1 2	32 54	-1
1 2	34 56	-1
1 2	36 58	-1
1 2	38 60	-1

Table 3: (continued)

$u^x_{ij} = -1$	$u^z_{ij} = -1$	parity
1 2	40 62	-1
1 2	42 64	-1
1 2	67 45	-1
1 2	47 69	-1
1 2	49 71	-1
1 2	51 73	-1
1 2	53 75	-1
1 2	55 77	-1
1 2	57 79	-1
1 2	59 81	-1
1 2	61 83	-1
1 2	63 85	-1
1 2	65 87	-1
1 2	88 66	-1
1 2	68 90	-1
1 2	70 92	-1
1 2	72 94	-1
1 2	74 96	-1
1 2	76 98	-1
1 2	78 100	-1
1 2	80 102	-1
1 2	82 104	-1
1 2	84 106	-1
1 2	86 108	-1
1 2	111 89	-1
1 2	91 113	-1
1 2	93 115	-1
1 2	95 117	-1
1 2	97 119	-1
1 2	99 121	-1
1 2	101 123	-1
1 2	103 121	-1
1 2	105 127	-1
1 2	107 129	-1
1 2	109 131	-1
1 2	132 110	-1
1 2	112 134	-1
1 2	114 136	-1
1 2	116 138	-1
1 2	118 140	-1
1 2	120 142	-1
1 2	122 144	-1
1 2	124 146	-1
1 2	126 148	-1
1 2	128 150	-1
1 2	150 152	-1
1 2	124 146	-1
1 2	155 133	-1
1 2	135 157	-1
1 2	127 159	-1
1 2	139 161	-1
1 2	141 163	-1

Table 3: (continued)

$u_{ij}^{x} = -1$	$u_{ij}^{z} = -1$	parity
1 2	143 165	-1
1 2	145 167	-1
1 2	147 169	-1
1 2	149 171	-1
1 2	151 173	-1
1 2	153 175	-1
1 2	176 154	-1
1 2	156 178	-1
1 2	158 180	-1
1 2	160 182	-1
1 2	162 184	-1
1 2	164 186	-1
1 2	166 188	-1
1 2	168 190	-1
1 2	170 192	-1
1 2	172 194	-1
1 2	174 196	-1
1 2	199 177	-1
1 2	179 201	-1
1 2	191 203	-1
1 2	183 205	-1
1 2	185 207	-1
1 2	187 209	-1
1 2	189 211	-1
1 2	191 213	-1
1 2	193 215	-1
1 2	195 217	-1
1 2	197 219	-1
1 2	220 199	-1
1 2	200 222	-1
1 2	202 224	-1
1 2	204 226	-1
1 2	206 228	-1
1 2	210 232	-1
1 2	212 234	-1
1 2	214 236	-1
1 2	216 238	-1
1 2	218 240	-1